The RT–PCR products obtained were directly sequenced and compared with a normal MPO cDNA sequence (Johnson et al., 1987; Morishita et al., 1987; Yamada et al., 1987). A guanine (G) to adenine (A) substitution was found in exon 9 region of the patient cDNA. This point mutation was located at position 1051 from adenine of first ATG (Fig. 2) and resulted in an amino acid conversion from glycine (GGC) to serine (AGC), G501S.

Genomic DNA for the MPO coding region and 5′ promoter region of the patient and his mother were amplified and sequenced to confirm the base substitution of the allele. The G to A substitution in exon 9 shown in Fig. 2b, was homozygous in the patient, but heterozygous in the patient's mother. This same exon was successfully sequenced and analyzed in 96 genomic DNA samples from healthy Japanese controls; sequencing for two of the original 98 controls was unsuccessful. None of these samples exhibited the G1051A mutation (Table 3). Analysis of the 5′ promoter region (− 463 from the first ATG), a polymorphic site, of patient, his mother and simultaneously prepared control samples revealed a homozygous guanine at that site (data not shown).

Table 3
Base substitutions of MPO gene

Source	Position of base substitution	
	5′ flanking region	Exon 9
	− 463	1051
Referred nucleotide*	A	G
Patient	G/G	A/A
Mother	G/G	A/G
Healthy control	G/G	G/G
Controls ($N=96$)	83% G/G 15% G/A 1% A/A	100% G/G

*Nucleotides from Genbank accession nos. X04876 and X15377.

4. Discussion

A single base substitution has been identified in the MPO cDNA in a patient with complete MPO deficiency. This G1051A mutation resulted in an amino acid change (G501S), which may have resulted in the said deficiency of the patient (Fig. 3). We could not detected mature MPO subunits (heavy and light subunit), although by Western blot analysis, we could detect 90-kDa prepro-MPO, which is the precursor of mature MPO subunits. The MPO mRNA from the patient did not reveal any alternative splicing sites and deletions. The − 463 G/A polymorphic site did not appear to play a role in this MPO deficiency, since there was no base difference between the patient and the 96 controls. Additionally, the allele frequency among the controls complied with data previously reported in the Japanese population with a predominance of the G/G genotype at that site (Hamajima et al., 2002) (Table 3).

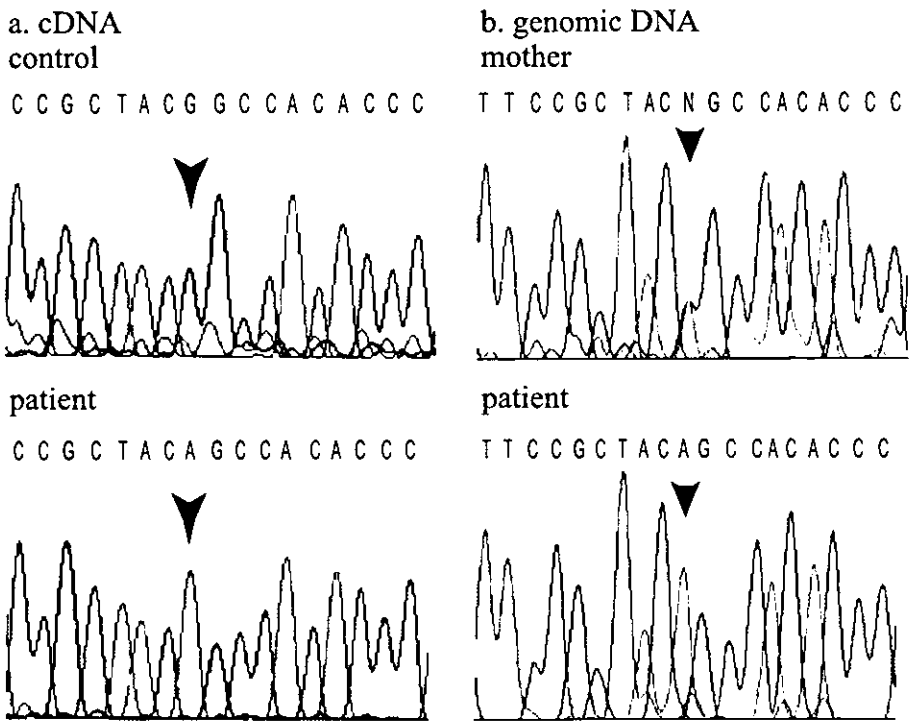

Fig. 2. Sequence histogram around the mutation point of cDNA and genomic DNA. (a) cDNA sequence of the patient and healthy control. The mutation position of 1051 was indicated with arrow heads. (b) Same coding region in genomic DNA of the patient and his mother.

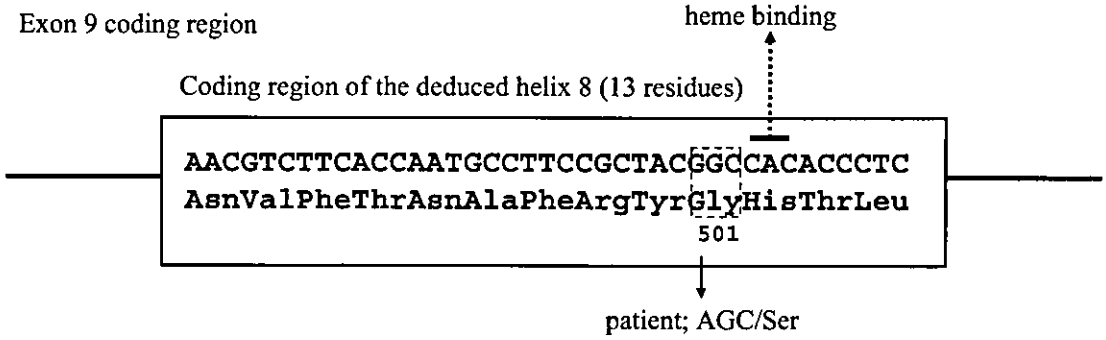

Fig. 3. Schematic diagram of exon 9. Amino acid residues and base sequence of deduced helix 8 region was shown in the box. G1051A causes amino acid substitution glysine to serine. His502 is a heme binding residue.

Three missense mutations on MPO gene which causes MPO deficiency, R569W (Nauseef et al., 1994, 1996), Y173C (DeLeo et al., 1998) and M251T (Romano et al., 1997) have been reported. Mature subunits of the enzyme are not formed in cases with R569W and Y173C mutation because posttranslational processing cannot be carried out correctly. M251T causes mature subunit but lacks enzymatic activity. The histidine at codon 502 (H502), which is included in the eighth helix domain constituting one part of heme-binding pocket, provides proximal ligand to the heme iron (Zeng and Fenna, 1992; Davey and Fenna, 1996). The missense mutation G501S is located adjacent to H502, also included in the eighth helix. The glycine to serine substitution possibly influenced the surrounding molecular environment of amino acid residues, especially the neighboring histidine residue, which plays an important role in heme binding. Thus, the G501S could cause an arrest in heme binding, an essential step for maturation of the enzymatically active MPO.

References

Aratani, Y., Koyama, H., Nyui, S., Suzuki, K., Kura, F., Macda, N., 1999. Severe impairment in early host defense against *Candida albicans* in mice deficient in myeloperoxidase. Infect. Immun. 67, 1828–1836.

Aratani, Y., Kura, F., Watanabe, H., Akagawa, H., Takano, Y., Suzuki, K., Maeda, N., Koyama, H., 2000. Differential host susceptibility to pulmonary infections with bacteria and fungi in mice deficient in myeloperoxidase. J. Infect. Dis. 182, 1276–1279.

Davey, C.A., Fenna, R.E., 1996. 2.3 A resolution X-ray crystal structure of the bisubstrate analogue inhibitor salicylhydroxamic acid bound to human myeloperoxidase: a model for a prereaction complex with hydrogen peroxide. Biochemistry 20;35 (33), 10967–10973.

DeLeo, F.R., Goedken, M., McCormick, S.J., Nauseef, W.M., 1998. A novel form of hereditary myeloperoxidase deficiency linked to endoplasmic reticulum/proteasome degradation. J. Clin. Invest. 101, 2900–2909.

Gullberg, U., Andersson, E., Garwicz, D., Lindmark, A., Olsson, I., 1997. Biosynthesis, processing and sorting of neutrophil proteins: insight into neutrophil granule development. Eur. J. Haematol. 58, 137–153.

Hamajima, N., Saito, T., Matsuo, K., Suzuki, T., Nakamura, T., Matsuura, A., Okuma, K., Tajima, K., 2002. Genotype frequencies of, 50, polymorphisms for, 241 Japanese non-cancer patients. J. Epidemiol. 12, 229–236.

Hashinaka, K., Nishio, C., Hur, S.J., Sakiyama, F., Tsunasawa, S., Yamada, M., 1988. Multiple species of myeloperoxidase messenger RNAs produced by alternative splicing and differential polyadenylation. Biochemistry 27, 5906–5914.

Johnson, K.R., Nauseef, W.M., Care, A., Wheelock, M.J., Shane, S., Hudson, S., Koeffler, H.P., Selsted, M., Miller, C., Rovera, G., 1987. Characterization of cDNA clones for human myeloperoxidase: predicted amino acid sequence and evidence for multiple mRNA species. Nucleic Acids Res. 15, 2013–2028.

Kawai, Y., Okawarab, A.I., Okuyama, H., Kura, F., 2000. Modulation of chemotaxis, O2-production and myeloperoxidase release from human polymorphonuclear leukocytes by the ornithine-containing lipid and serineglycine-containing lipid of *Flavobacterium*. FEMS Immunol. Med. Microbiol. 28, 205–209.

Laemmli, U.K., 1970. Cleavage of structural proteins during the assembly of the head of bacteriophage T4. Nature 15;227 (259), 680–685.

Lanza, F., 1998. Clinical manifestation of myeloperoxidase deficiency. J. Mol. Med. 76, 676–681.

Minoshima, S., Arimura, Y., Nakabayashi, K., Kitamoto, K., Nagasawa, T., Okawara, A.I., Suzuki, K., 1997. Increased release of myeloperoxidase in vitro from neutrophils of patients with myeloperoxidase-specific antineutrophil cytoplasmic antibody (MPO-ANCA) related glomerulonephritis. Nephrology 3, 527–534.

Morishita, K., Kubota, N., Asano, S., Kaziro, Y., Nagata, S., 1987. Molecular cloning and characterization of cDNA for human myeloperoxidase. J. Biol. Chem. 262, 3844–3851.

Nauseef, W.M., Brigham, S., Cogley, M., 1994. Hereditary myeloperoxidase deficiency due to a missense mutation of arginine, 569, to tryptophan. J. Biol. Chem. 269, 1212–1216.

Nauseef, W.M., Cogley, M., McCormick, S., 1996. Effect of the R569W missense mutation on the biosynthesis of myeloperoxidase. J. Biol. Chem. 271, 9546–9549.

Nauseef, W.M., Cogley, M., Bock, S., Petrides, P.E., 1998. Pattern of inheritance in hereditary myeloperoxidase deficiency associated with the R569W missense mutation. J. Leukoc. Biol. 63, 264–269.

Nunoi, H., Kohi, F., Kajiwara, H., Suzuki, K., 2003. Prevalence of inherited myeloperoxidase deficiency in Japan. Microbiol. Immunol. 47, 527–531.

Reynolds, W.F., Stegeman, C.A., Cohen Tervaert, J.W., 2002. −463 G/A Myeloperoxidase promoter polymorphism is associated with clinical manifestations and the course of disease in MPO-ANCA-associated vasculitis. Clin. Immunol. 103, 154–160.

Romano, M., Dri, P., Dadalt, L., Patriarca, P., Baralle, F.E., 1997. Biochemical and molecular characterization of hereditary myeloproliferative deficiency. Blood 90, 4126–4134.

Suzuki, K., Ota, H., Sasagawa, S., Sakatani, T., Fujikura, T., 1983. Assay method for myeloperoxidase in human polymorphonuclear leukocytes. Anal. Biochem. 132, 345–352.

Suzuki, K., Yamada, M., Akashi, K., Fujikura, T., 1986. Similarity of kinetics of three types of myeloperoxidase from human leukocytes

and four types from HL-60 cells. Arch. Biochem. Biophys. 245, 167–173.

Suzuki, K., Nunoi, H., Miyazaki, M., Koi, F., 2000. Prevalence of inherited myeloperoxidase deficiency in Japan. In: Petrides, P.E., Nauseef, W.M. (Eds.), The Peroxidase Multigene Family of Enzymes. Springer-Verlag, Berlin, pp. 145–149.

Yamada, M., Hur, S.J., Hashinaka, K., Tsuneoka, K., Saeki, T., Nishio, C., Sakiyama, F., Tsunasawa, S., 1987. Isolation and characterization of a cDNA coding for human myeloperoxidase. Arch. Biochem. Biophys. 255, 147–155.

Zeng, J., Fenna, R.E., 1992. X-ray crystal structure of canine myeloperoxidase at 3 A resolution. J. Mol. Biol. 226, 185–207.

Available online at www.sciencedirect.com
SCIENCE DIRECT®
Biochemical and Biophysical Research Communications 314 (2004) 46–53
BBRC
www.elsevier.com/locate/ybbrc

Applications of T-lymphoma labeled with fluorescent quantum dots to cell tracing markers in mouse body

Akiyoshi Hoshino,[a,b] Ken-ichi Hanaki,[a] Kazuo Suzuki,[b] and Kenji Yamamoto[a,*]

[a] *Department of Medical Ecology and Informatics, Research Institute, International Medical Center of Japan, 1-21-1 Toyama, Shinjuku, Tokyo 162-8655, Japan*
[b] *Department of Bioactive Molecules, National Institute of Infectious Diseases, 1-23-1 Toyama, Shinjuku, Tokyo 162-8640, Japan*

Received 25 November 2003

Abstract

Photoluminescent semiconductor quantum dots (QDs) are novel nanometer-size probes that have found bioimaging. Here we imaged a cell line of mouse lymphocytes. QDs were actively taken into the target cells by endocytotic pathways. The fluorescence of QDs held in the endosomes could be studied for more than a week and remained stable luminescence against cell activation induced by concanavalin A, phytohemagglutinin, phorbol myristate acetate, and calcium ionophore A23187. These results suggested that QD-labeling was stable and did not affect either cell activation or cell function. When QD-labeled cells were intravenously injected into mouse, they remained in the peripheral blood in a concentration of approximately 10% up to 5 days after injection using both fluorescence microscopy and flow cytometry. In addition, approximately 20% of QDs were detected in the kidneys, liver, lung, and spleen and could still be observed 7 days after injection. These results suggested that fluorescent probes of QDs might be useful as bioimaging tools for tracing target cells over the period of a week in vivo.

Keywords: Bioimaging; Cell labeling marker; Cytotoxicity; In vivo; Living cell; Quantum dot; Semiconductor

Ultrafine nanocrystals are expected to be used widely in biotechnology and medical applications for separating biomaterials, immunoassay, diagnostics, and drug-carriers that are applied to the drug delivery systems [1–6]. Quantum dots (QDs) are novel inorganic fluorophores that consist of CdSe/ZnS-core/shell semiconductor nanocrystals. QDs have several advantages over organic fluorophores. QDs show high luminance, resistance to photobleaching, a range of excitement wavelengths from ultraviolet to red that depend on the size of the particles, and cover a range of fluorescent wavelengths from blue to red that can be excited using a mercury arc lamp [7,8]. At present, many organic fluorophores such as fluorescein isothiocyanate (FITC) and carboxyfluorescein diacetate succinimidyl ester (CFSE) have been used in various biological applications, such as fluorescent-labeled antibodies and molecules that are used to stain cells or cellar organs [8,9]. Experiments using organic dyes are limited to short-time assays such as flow cytometry due to the lifetime of fluorescence. Those dyes were not suitable for extended periods of bioimaging observations using fluorescent and confocal microscopy because organic fluorophores tend to quench rapidly [6,10]. Furthermore, it is sometimes difficult or impossible to record fine fluorescent images while the organic coloring probes fade in the course of adjusting the focus. In contrast, QDs are stabilized over a far longer exposure-time to light and can emit a fluorescence of high luminosity at an almost equivalent condition as the conventional organic fluorescence probes.

Initially, chemically synthesized QDs have not been applied to biochemical applications because they do not dissolve in water. Since hydrophilic surface treatment of QD was developed, the application range of QDs has been rapidly spreading to bioimaging [11–13]. However, QDs can easily aggregate at acidic- and even in isotonic-conditions because they are unstable in either acidic or saline conditions. Hence, QD-conjugated biomolecules are difficult to produce because most of the biomolecules

* Corresponding author. Fax: +81-3-3202-7364.
E-mail address: backen@ri.imcj.go.jp (K. Yamamoto).

0006-291X/$ - see front matter © 2003 Elsevier Inc. All rights reserved.
doi:10.1016/j.bbrc.2003.11.185

exist in the isotonic condition in vivo [14]. The molecules that can conjugate with QDs are few: streptavidin, oligopeptides, and some antibodies [13,15,16]. We have considered methods to stabilize QDs in biological solutions such as culture media [11,17]. We previously examined albumin from 10 species to assess efficient stabilization since QDs could be conjugated to albumin non-specifically [17]. Time-lapse study of the intracellular distribution of QDs in culture cells has already been performed and the endosomal vesicles including QDs were observed [17]. In this study we assessed whether QDs could be applied to various applications using labeled cells for the purpose of long-time tracing. Labeled concentration of QDs did not appear to show any signs of cytotoxicity. Although there are many applications where QDs are used as dyes to stain mammalian cells and bacteria in vitro [17,18], no applications have been demonstrated where QDs can be used in cells that are transplanted into the living animals.

Materials and methods

Reagents and preparation of albumin-conjugated QDs. CdSe/ZnS-core/shell QDs (fluorescence wavelength: 520 nm) were conjugated with sheep serum albumin fraction V (Sigma) according to our study, as previously reported [17]. Briefly, albumin-conjugated QDs were prepared by mixing equal volumes of QD-sodium salt solution (10 mg/ml) and sheep albumin solution (10 mg/ml) in the presence of EDC (1-ethyl-3-[3-dimethylaminopropyl]carbodiimide hydrochloride) coupling reagents purchased from Pierce Biochemical. The mixture was incubated for 30 min at room temperature and applied to a Sephadex G-25 column (Amersham Biosciences) to remove the excess fraction of reagents. The QD-working solution was prepared by diluting the QD-mixture with DMEM/F-12 culture media (Gibco), immediately filtered with a 0.1-μm centrifuge membrane filter (Millipore, Ultrafree-MC), and centrifuged at 10,000*g* for 10 min before use.

Assessment of QD-Uptake by cells. EL-4 cells, which were established from murine T-cell lymphoma, were cultured in DMEM/F12 supplemented with 5% heat-inactivated fetal bovine serum at 37 °C. The cells were plated at a volume of 1×10^6 cells/well on a 12-well culture plate (Iwaki) and were stimulated with the indicated concentration of QDs. After incubation, the cells were harvested and washed with phosphate-buffered saline (PBS) twice to remove the non-specific binding QDs. The cells were stained with 100 μg/ml propidium iodide solution. Then the cells were fixed with 10%-formaldehyde neutral buffer. As many as 1×10^6 cells were analyzed by flow cytometer (JASCO CytoAce300). Fluorescence was excited using argon laser (488 nm). Detection was triggered by forward-angle light-scattered signals at wavelength of 520 nm. Images were acquired with a digital camera D1X (Nikon) on a fluorescent microscope IX-81 (Olympus) using WIBA mirror unit to adjust the excitation wavelength to 470–490 nm and oil immersion objective lens.

Mice and separation of the cells and organ. BALB/c AnNCrj-nu/nu (nude) mice (5w, male) were purchased from Charles River Japan Inc. EL-4 cells used for administration were pre-stained with a PKH26 Red Fluorescent Cell Linker Kit purchased from Sigma before stimulation with albumin-conjugated QDs. The cells holding QDs were collected 2 h after stimulation and resuspended to the concentration of 5×10^7 cells/ml in serum-free DMEM/F12. Two hundred microliters of cell-suspended solution was intravenously injected to mice. The mice were sacrificed 2 h, 1 day, 3 days, 5 days, and 7 days after injection and the peripheral blood was collected. The blood was laid onto a Ficoll–Metrizoate density gradient (Histopaque-1083 solution, Sigma) and centrifuged at 700*g* for 30 min at room temperature to form a distinct layer at the plasma-media interface. The leukocyte fraction including EL-4 cells was separated from the interface of the two solutions. Then contaminated erythrocytes were removed by 2 washes in ACK-lysis buffer (150 mM NH_4Cl, 1 mM $KHCO_3$, and 0.1 mM EDTA, pH 7.4). Each lysis was performed by incubating for 5 min at room temperature followed by washing the cells with PBS twice. Fluorescence intensity of QD-holding cells was detected by flow cytometric analysis and by fluorescent microscopy.

Collected kidney, liver, lung, and spleen organs were immediately washed three times by PBS to remove retained erythrocytes. Then each organ was incubated with 4% paraformaldehyde for 2 h at room temperature. After soaking, the organs were washed and incubated with 70% ethanol at 4 °C overnight. After embedding into paraffin, the section was sliced to 10 μm thickness. The section was affixed to slide glass (Matsunami).

Results and discussion

Many researchers have applied various techniques to recognize the introduced target cells specifically; labeled cells directly with organic fluorophores like CFSE [8,9], dyed X–Y chromosome by fluorescence in situ hybridization (FISH) using sex-mismatched target cells [19], transformed the gene coded specific molecule like green fluorescent proteins (GFPs), various kind of luciferases, or some cell surface expression molecules, etc. [20,21]. But unfortunately, it gets hanged up and it is costly to detect the target cells by these procedures. To remove those problems, we assessed the possibility of using QDs as the markers for the introduced target cells in vivo. First, we examined how long it took for the EL-4 cells to take up the albumin-conjugated QDs. EL-4 cells were plated at 1×10^6 cells/well and stimulated with 0.1 mg/ml QDs for 15, 30, and 60 min at 37 °C. Shown in Fig. 1A, the QDs were adherent to the cell surface 15 min after incubation. The vesicles including QDs started to form 30 min after incubation and QDs were recruited into the cellular granules after 60 min. We assumed that this uptake would be inhibited at chilled conditions if it were performed via endocytotic pathways. To investigate whether this uptake reaction was dependent on their temperature, EL-4 cells were cultured with QDs at chilled condition. As expected, QDs were also found adhering to the cell surface, but uptake into the cell vesicles was blocked even after 60 min incubation (Fig. 1A). In addition, re-incubating the cells at 37 °C, the QD uptake into the cells recovered again (Fig. 1B). This adhesion is not detached by washing the QD-holding cells and fluorescence of the cells was measured by flow cytometry, which was the same as at 37 °C conditions. These results suggested that uptake of QDs into the cells occurs via endocytotic pathways. This indicated that processing for 15 min to stain the cell surface is sufficient for the purpose of short-time cell tracing. Thus, QDs can become an effective cell marker for several days after only short-time treatment of the cell.

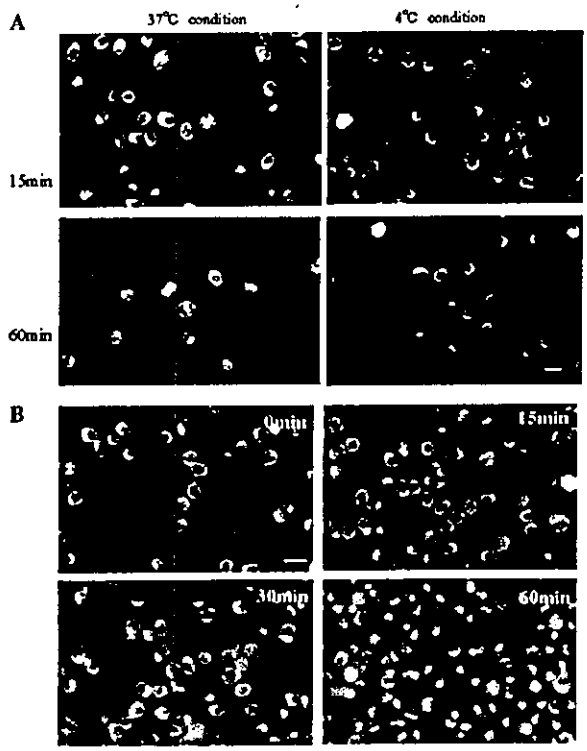

Fig. 1. Uptake of albumin-conjugated QD by EL-4 cells was dependent on temperature. (A) EL-4 murine lymphocytoma cells were plated and stimulated with albumin-conjugated QD at the concentration of 0.1 mg/ml and incubated for 15 and 60 min at 37 and 4 °C conditions. QD- labeled cells were observed by fluorescent microscopy. The bright green granules indicated fluorescence emitted from QDs. (B) Cells were pre-incubated for 20 min before stimulation. Then the cells were stimulated with QDs for 60 min at 4 °C condition and re-incubated at 37 °C for the indicated time. Bars indicate 10 μm. In all the figures, the observation data represent one out of three performed.

When QDs were used as long-term tracing markers, the acute cytotoxicity of QDs raises a problem. To investigate the relation between concentration and cytotoxicity of QDs, we assessed the cell viability after QD-stimulation. The cells were cultured at the concentration of 0.1, 0.2, and 0.4 mg/ml of QDs for 24 h and stained with propidium iodide to detect dead cells. As the fluorescence intensity of QD-holding cells increased by the concentration of QDs, the number of dead cells also increased (Fig. 2). The cytotoxicity was observed in proportion to the concentration of QDs and almost all of the cells were dead at 0.4 mg/ml more than 6 h after incubation. However, no remarkable cytotoxicity was observed at 0.1 mg/ml. Since using a high-concentration of QDs induced the cell death, we decided to use QDs at 0.1 mg/ml concentration.

Next we also examined how long QDs could be retained in the cells. To investigate this, EL-4 cells were further cultured after stimulation with QDs. Cell growth of EL-4 cells was choked by stimulation with QDs even

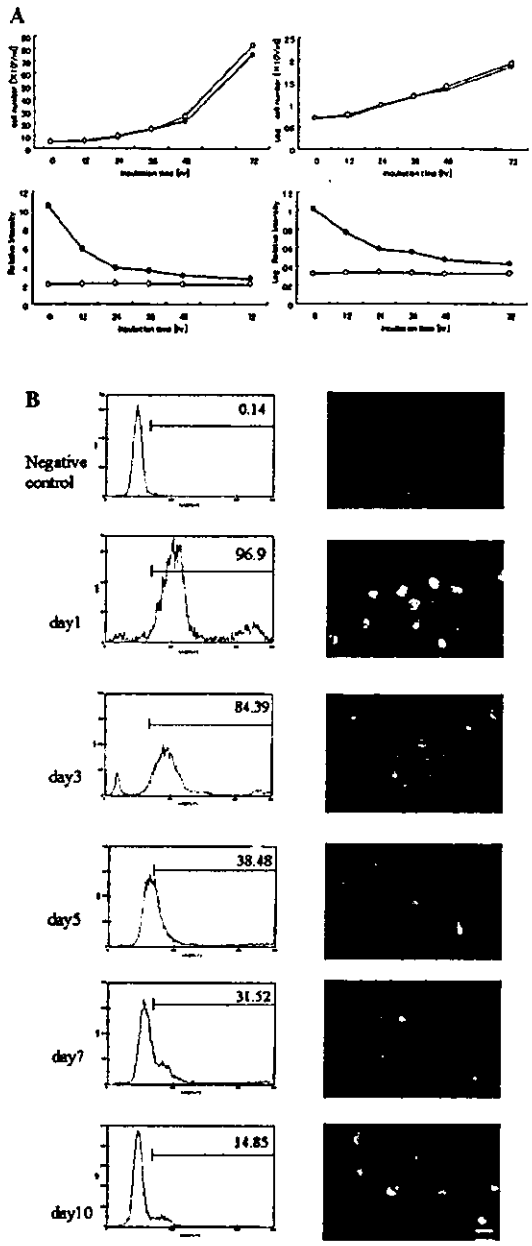

Fig. 3. QDs labeled on EL-4 cells were observed more than a week in vitro. (A) The *upper graphs* show a comparison between the growth curve of the unlabeled and QD-labeled EL-4 cells; open circles indicated the number of control cells and the closed circles are the QDs, respectively. The *lower graphs* show the relative fluorescence intensity of 10^5-collected cells measured by spectrofluorometer (JASCO, FP-6500); open circles indicated the fluorescence intensity of the control cells and the closed circles are the QDs, respectively. Each Graph in *right lanes* shows the logarithmic scales corresponding to the *left* ones. The data are presented as means ± standard deviation. (B) EL-4 cells were stimulated with QDs at 0.1 mg/ml concentration. The cells were incubated for 1, 3, 5, 7, and 10 days. The cells were harvested, stained with propidium iodide for detection of dead cells, and observed by flow cytometry and fluorescent microscopy, as in Fig. 1. The fluorescence intensity of the QD-holding cells in 10^6-collected cells was measured by flow cytometric analysis and the cell population in each region was calculated by CytoAce300 analyzer (JASCO).

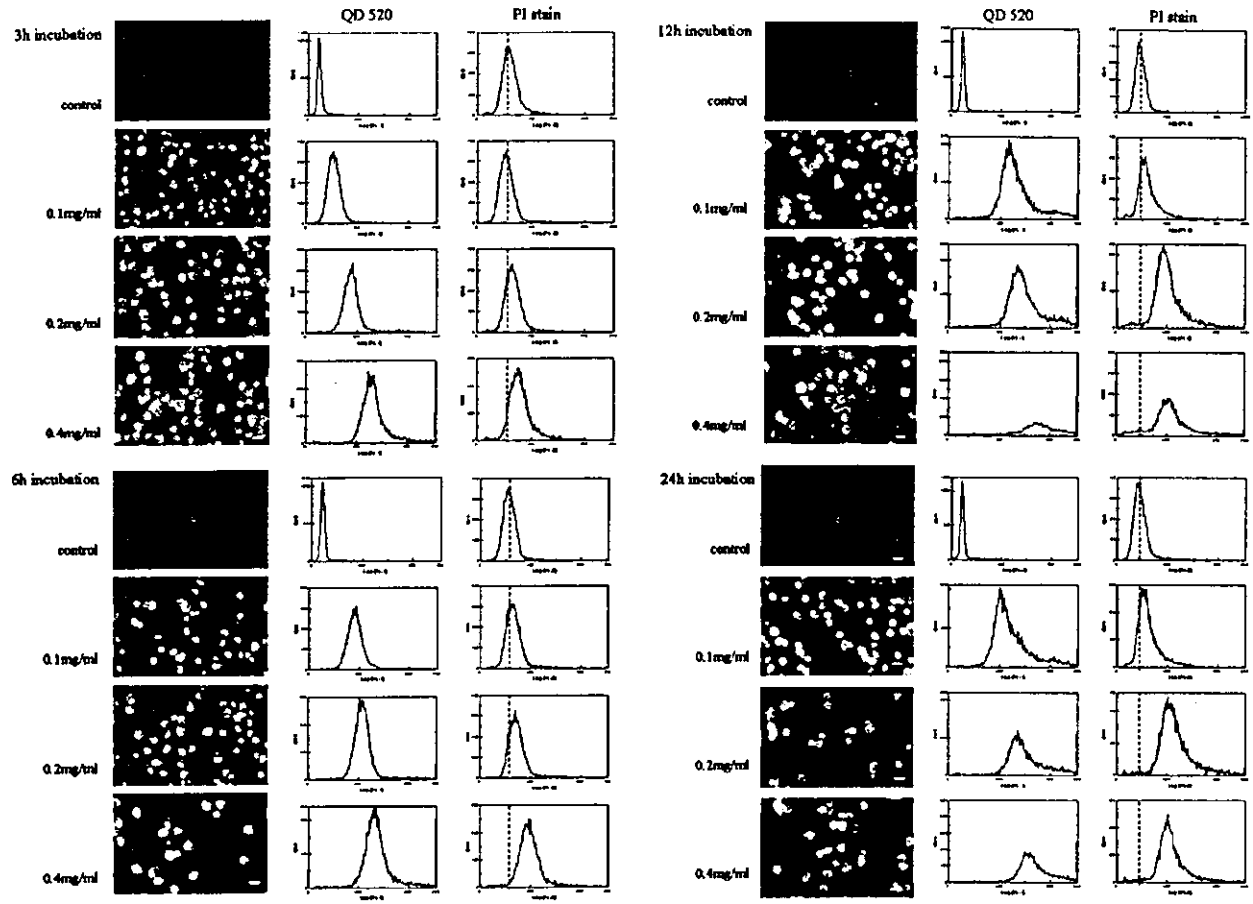

Fig. 2. The cytotoxicity of albumin-conjugated QDs depends on the QD-concentration. EL-4 cells were stimulated with culture media alone or with albumin-conjugated QD at the concentration of 0.1, 0.2, and 0.4 mg/ml. Cells were incubated for 3, 6, 12, and 24 h at 37 °C. The cells were harvested, stained for observation of dead cells, and measured by flow cytometric analysis. Fluorescence was measured by flow cytometry using an argon laser (488 nm). Detection was triggered by forward-angle light scattered signals. In the *graphs*, the relative cell number is given on the *y*-axis and the fluorescence intensity of QDs on the *x*-axis. Dotted lines in the *graphs* indicate the fluorescence medium of the unstimulated cells.

in 0.1 mg/ml concentration (Fig. 3A, upper graphs). Whereas the growth of both cells conformed to logarithmic growth phase, the doubling-time of QD-labeled cells was about 24 h and took 4 h longer than unlabeled cells (approximately 20 h). The fluorescence intensity of QD-labeled cells was logarithmically attenuated, but the attenuation ratio became lower after 24 h incubation (Fig. 3A, lower right). Moreover, the QDs that remained in the cells could be observed for more than a week (Fig. 3B). Approximately 10% of the cells still held QDs after 10 days culture, but fluorescent intensity of cells gradually decreased and highly concentrated in endosomes. This concentration of QDs was compatible with our previous study in Vero cells [17], implying that this labeling of cells by QDs could be applied not only adherent cell but also the cells that have the property of less endocytotic action and high-proliferation rate cells such as lymphocytes.

It is known that T cells were activated with various immune stimulants. Then, we investigated whether labeling of QDs held in the cells would be influenced by those stimulations. EL-4 cells were exposed to various stimulants after labeling of QDs. After stimulation, EL-4 cells were highly aggregated by stimulation with ConA and PHA. But no significant change was observed by stimulating for 24 h (Fig. 4). These results suggest that labeling of QDs were stable, and were not affected by either cell activation or cell function.

Then we compared the fluorescence of QD with those of other organic probes at the points of fluorescence intensity and photostability. Shown in Fig. 5A, fluorescence intensity of both QD and organic probes was approximately equivalent in the moment of excitation in the case of flow cytometric analysis. However after long-term exposure, e.g., long time observation using microscopes, fluorescence from organic probes was eliminated rapidly and almost disappeared within a minute (Fig. 5B). In contrast, the QDs kept emitting bright fluorescence for more than 30-min continuously (Fig. 5C).

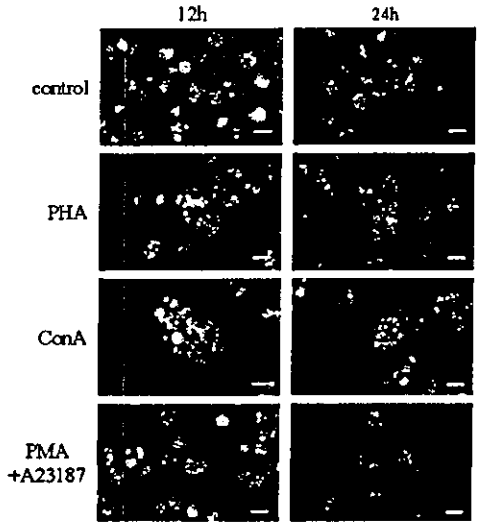

Fig. 4. Fluorescence of QDs was stable against activation of EL-4 cells. EL-4 cells were incubated with QD at 0.1 mg/ml concentration for 3 h. Then the cells were washed twice with DMEM and stimulated with 1 μg/ml ConA, 5 μg/ml PHA, and both 10 ng/ml PMA and 1 μM A23187. The cells were collected 12 and 24 h after stimulation. The cells were observed using a fluorescent microscopy, as in Fig. 1.

Next we considered the survival of QD-labeled cells in vivo. The cells labeled by QDs were intravenously injected into mice. The cells injected into mice were observed in the peripheral blood for 5 days after injection by microscopic analysis (Fig. 6). The fluorescence of QD-labeled cells was also observed until 5 days after injection, but the fluorescence intensity of cells was much smaller than expected. Unfortunately, fluorescence of PKH-dye was observed from cells by using neither microscopy nor flow cytometric analysis (data not shown). However, approximately 70% of QD-labeled cells were eliminated from blood circulation within 2 h after injection. We assumed that the excess number of QD-labeled cells would be homing on the other lymphatic tissue, as T-cell population in whole peripheral blood usually remained at approximately 20%. As expected, many cells including QDs were observed in spleen sections at 2 h after injection (Fig. 7A). In 2 h images, QD-labeled cells remained in the fringe area of white pulp and red pulp. After 5 days, fluorescence emitted from QDs was located in white pulp area. This result concurs with the fact that T-lymphocytes were first observed in red pulp and then moved and then

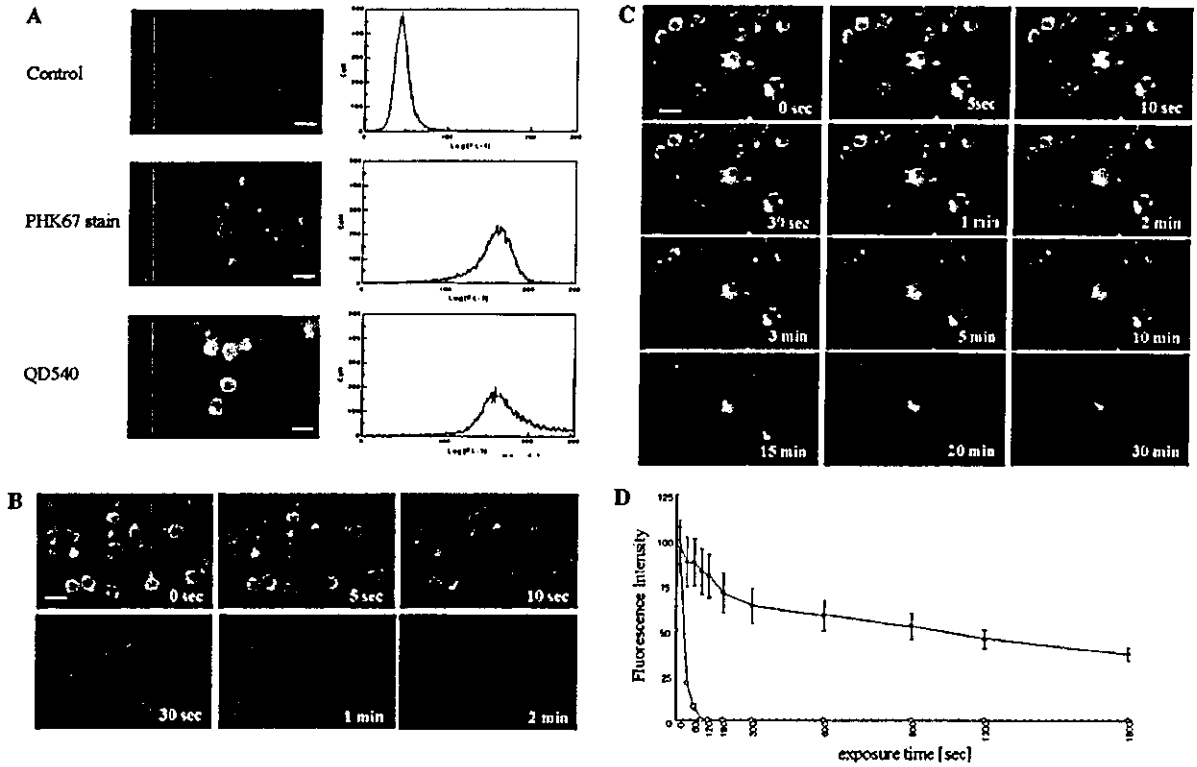

Fig. 5. Fluorescence of QDs was superior to that of organic flourophores with respect to the fluorescent lifetime. (A) Cells stained with QDs and organic dyes were observed by fluorescent microscopy and flow cytometric analysis. The cells were harvested, stained, and analyzed by flow cytometry and fluorescent microscopy, as in Fig. 1. (B) Observation of photostability of organic probe (PHK67). The cells were continuously excited and images were taken using D1X digital camera equipped with fluorescence microscope IX-81 at the indicated time by a 1.0 s exposure. Other conditions were the same as described in Fig. 1. (C) The photostability of QDs, as described in (B). (D) Comparison of the relative fluorescence intensity between QDs and the organic probes. The snapshots shown in Figs. 3B and C were calculated using the histogram analysis of Adobe Photoshop 7.0. Open circles indicate organic probes and closed circles are the QDs, respectively.

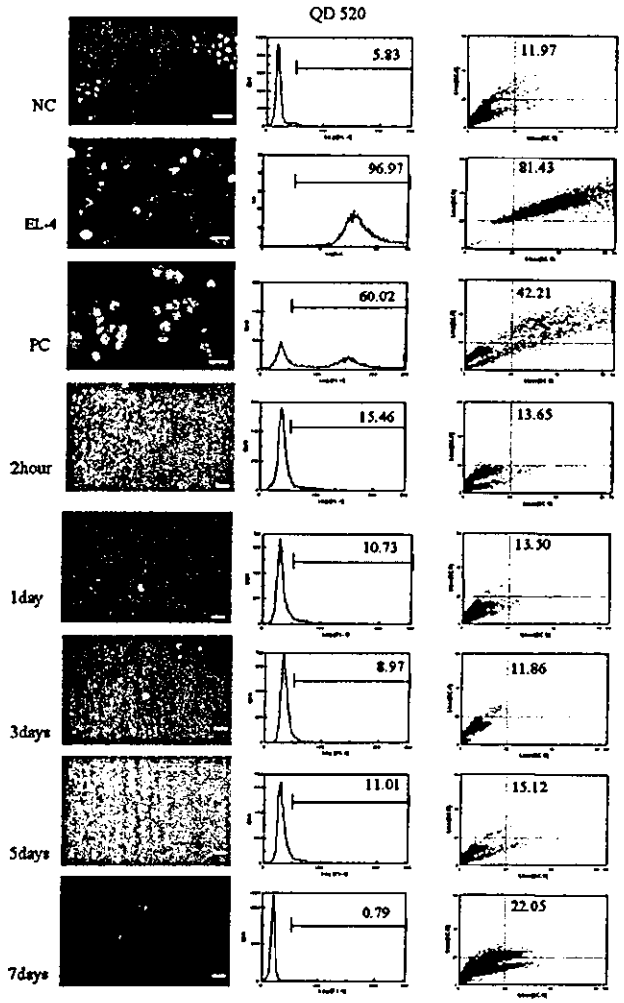

Fig. 6. Intravenously injected QD-labeled cells remained for several days in the peripheral blood. EL-4 cells used for administration were pre-stained with PKH26 Red Fluorescent Cell Linker Kit (Sigma) before incubated with 0.1 mg/ml QD. Then the cells were collected and re-suspended in serum-free DMEM and intravenously injected into the mice. The mice were sacrificed at indicated days ($n = 2$). The fluorescence intensity of the QD-holding cells was measured and calculated by a CytoAce300 analyzer, as shown in Fig. 3. In the *right graphs*, the forward scattered is given on the *y*-axis and side scattered on the *x*-axis. Shown numbers in inset mean the percentage of cells in upper right region of graphs. As positive control, an equivalent number of QD-labeled cells were added into the blood separately.

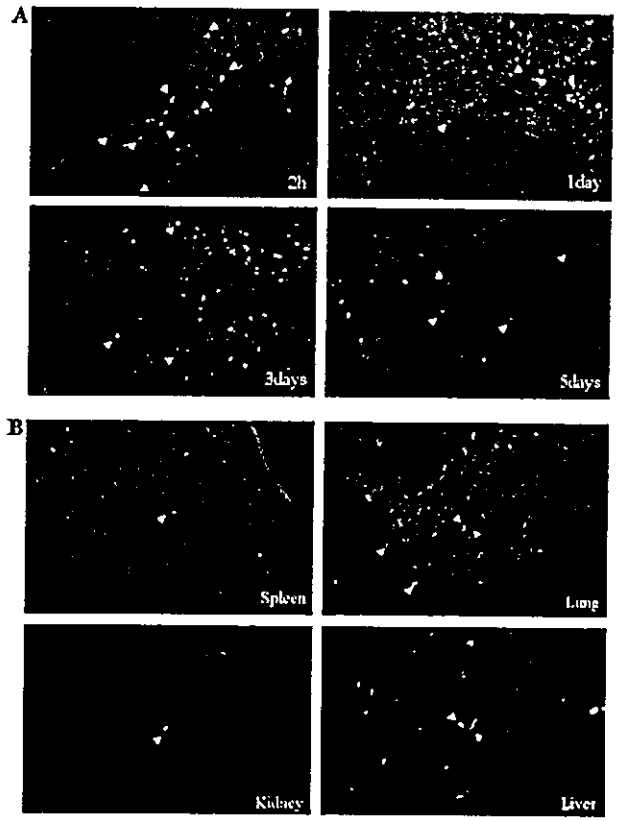

Fig. 7. QD-labeled EL4 was located into kidney, liver, lung, and spleen. (A) The fluorescence images of sliced spleen collected 2 h, 1 day, 3 days, and 5 days after administration ($n = 2$). (B) The fluorescence images of the kidneys, liver, lung, and spleen 7 days after administration. The cells were observed by fluorescence microscopy, as in Fig. 1. Arrowheads indicate the location of QD-holding cells.

accumulated in the splenic white pulp. In addition, QD-labeled cells could be detected in sections of the kidneys, liver, and lung in 7 days (Fig. 7B). The estimated value of QDs in each organ calculated in accordance with QDs contained in each section is shown in Table 1. This result suggests that approximately 20% of injected cells were present in those organs 7 days after injection.

Our results suggested that the QDs could be used as a cell-tracing marker, especially for that of the transplanted target cells. QDs could enable high luminescent labeling of target cells easily and these applications could also be applied to flow cytometric analysis. In this study, we performed the labeling of QDs in EL-4 lymphocytoma cell lines by cellular endocytotic pathways. This result indicated that it is possible to tag target cells only by adding albumin-conjugated QDs into the culture media. In addition, the injected QD-labeled cells were observed up to 5 days in this experiment. However, some of the QDs were eliminated from the cells after a long-time incubation time even in vitro, and the observed number of cells was smaller than expected; the number of cells observed 2 h after injection was quarter of the anticipated value and it decreased to 1/6 by next day. It was not elucidated in this research why QD labeled cells were disappearing from the body in these experiments, but we can presume three possibilities by our study. The first possibility was the attenuation of QDs from endosomes by cell division. As shown in Fig. 3, labeled QDs have already been detached in most of the labeled cells, even though a few QD-labeled cells remained for over a week in vitro. The fluorescence intensity of QD-labeled cell population was attenuated within first 24 h, but fluorescent attenuation ratio

Table 1
The estimated number of injected cells labeled by QDs contained in each organ at indicated days after injection

Time	Organ	QD-labeled cells in each section (cells/section)	Estimated cell numbers in each organ ($\times 10^4$ cells/organ)
2 h	Spleen	605 ± 133	41.2 ± 13.4 (4.1%)
	Kidney	Not detected	Not detected
	Liver	1.0 ± 1.0	0.58 ± 0.63 (0.06%)
	Lung	46.7 ± 18.0	18.6 ± 71.9 (1.86%)
3 days	Spleen	97.7 ± 27.7	6.64 ± 2.44 (0.66%)
	Kidney	0.33 ± 0.58	0.04 ± 0.07 (0.004%)
	Liver	2.0 ± 1.0	1.16 ± 0.68 (0.12%)
	Lung	47.3 ± 5.0	18.5 ± 2.15 (1.85%)
7 days	Spleen	72.0 ± 10.8	4.90 ± 1.24 (4.9%)
	Kidney	1.3 ± 0.6	0.15 ± 0.09 (0.15%)
	Liver	10.6 ± 2.1	6.17 ± 1.75 (6.1%)
	Lung	51.6 ± 11.0	20.1 ± 4.52 (20.1%)

QD-labeled cells including each organ section were counted ($n = 3$). The estimated cell numbers in each organ were the presumed value calculated from the volume of the organs and the number of QD-labeled cells contained in the sections. The data are presented as means ± standard deviation. The value in parentheses shows the percentages of the injected QD-labeled cells located in each organ.

became lower after more than 24 h culture. Moreover, QDs held in endosomes were gradually concentrated in a time-dependent manner. The distribution of QDs may incline toward the specific position in a cell, which resulted in that QD may be unevenly distributed to the two product cells at cell division. Probably QDs may be eliminated from injected cells in the same way in vivo. Furthermore, the influence by cell division in the mouse cannot be disregarded either. As shown in Fig. 6, injected EL-4 cells were grown after 5 days (*right graphs*) and detection of QD-labeled cells became difficult 5 days after injection (*left graphs*). Thus, cell labeling using QDs may tend to be influenced by cell division. The second possibility was exclusion of injected cells by the host-immune system. QDs holding cells may be vanishing more rapidly out of the blood circulation by some active pathways in the early stage after injection. As we surmised that QDs were excluded by the spleen function, QD-labeled cells were detected from the sections of the kidneys, liver, lung, and spleen. Approximately 20% of injected QD-labeled cells were accumulated in those four organs up to 7 days after injection. The last possibility was the loss of photoluminescent ability of the QDs. It was known that the fluorescence emitted from QDs was attenuated by depriving of electric charge on QDs. We assumed that the degradation of the surface of QDs in endosomes including QDs was due to a change of the pH as a consequence of activation of T cells. But as shown in Fig. 4, no significant fluorescent elimination was observed although QD-holding lymphocytes were stimulated with calcium ionophore A23187, PMA, and some lectins such as ConA and PHA.

Our approaches suggest that QDs can be traced using the injected cells for more than a week by quite easy techniques. In this approach, QDs had many more advantageous points than organic fluorophores. As shown in Fig. 5, the fluorescent intensity of QDs was approximately equal to that of the organic fluorophores in short-time exposure such as flow cytometry, but the fluorescence of QDs was superior to that of organic fluorophores in terms of the operating lifetime. QDs could be applied not only to cell labeling marker but also to real-time single-molecule bioimaging for several minutes in living cells, such as antigen–antibody reactions, the moment of viral infection, the movement of transcription in nuclei, and more. More improvements may be achieved by multicolor scanning using some QDs of different particle sizes [22].

At present, no damage or toxicity caused by injection of QD-labeled cells over individuals was observed although the adverse effects on the organisms by the QDs were anticipated, and cytotoxicity was observed at high concentration of QDs. Efforts to address this issue are being made in developing a different silicon based QD. Further miniaturization of the particle is anticipated and silicon-based QDs are expected to be much safer because neither cadmium nor selenium is used. Advanced surface treatment and improved introducing-methods of QDs were required to retain the QDs inside the cells for a longer and more stable duration. Nowadays, another introduction method that encapsulated individual nanocrystals in liposomes is being considered [23–25]. QDs could be used in both carrier or drug delivery systems and to assess the effects of treatment by combining this method and the other gene targeting therapy using the liposomes if a semi-permanent cell labeling technique was enabled in those methods [26]. Furthermore, a small tumor can be detected by specific wavelength infrared rays emitted from some QDs, as the QDs can be conjugated with biomolecules which can specifically recognize tumor cells in a similar way as antibodies and some lectins [27]. Visualization of QDs which flowed in the blood of the capillary vessels and which were accumulated in adipose tissue has already been reported using multiphoton microscopy [28].

The dynamics of QDs in this application is dependent on the albumin conjugating on the surface of the QDs. Further, it may be expected to conjugate QDs with various proteins or molecules for the carrier molecules of drug delivery system or cell specific marker. With the development of new surface treatments of QDs, it may soon become possible to make these possibilities come true using various methods to replace the conventional organic fluorophores that are currently being used.

Acknowledgments

We are grateful to Drs. Tomokazu Nagao, Ken Murayama, and Wayne Dawson (National Institute of Infectious Diseases) for valuable advice and help with data collection, animal treatment, and proofreading. This work was supported by Grant 'H14-nano-004' of the Ministry of Health, Labor and Welfare of Japan.

References

[1] S.J. Rosenthal, I. Tomlinson, E.M. Adkins, S. Schroeter, S. Adams, L. Swafford, J. McBride, Y. Wang, L.J. DeFelice, R.D. Blakely, Targeting cell surface receptors with ligand-conjugated nanocrystals, J. Am. Chem. Soc. 124 (2002) 4586–4594.

[2] B. Dubertret, P. Skourides, D.J. Norris, V. Noireaux, A.H. Brivanlou, A. Libchaber, In vivo imaging of quantum dots encapsulated in phospholipid micelles, Science 298 (2002) 1759–1762.

[3] G.T. Shubeita, S.K. Sekatskii, G. Dietler, I. Potapova, A. Mews, T. Basch, Scanning near-field optical microscopy using semiconductor nanocrystals as a local fluorescence and fluorescence resonance energy transfer source, J. Microsc. 210 (2003) 274–278.

[4] H. Xu, M.Y. Sha, E.Y. Wong, J. Uphoff, Y. Xu, J.A. Treadway, A. Truong, E. O'Brien, S. Asquith, M. Stubbins, N.K. Spurr, E.H. Lai, W. Mahoney, Multiplexed SNP genotyping using the Qbead system: a quantum dot-encoded microsphere-based assay, Nucleic Acids Res. 31 (2003) 43.

[5] X. Wu, H. Liu, J. Liu, K.N. Haley, J.A. Treadway, J.P. Larson, N. Ge, F. Peale, M.P. Bruchez, Immunofluorescent labeling of cancer marker Her2 and other cellular targets with semiconductor quantum dots, Nat. Biotech. 21 (2003) 41–46.

[6] W.C. Chan, D.J. Maxwell, X. Gao, R.E. Bailey, M. Han, S. Nie, Luminescent quantum dots for multiplexed biological detection and imaging, Curr. Opin. Biotech. 13 (2002) 40–46.

[7] H. Mattoussi, J.M. Mauro, E.R. Goldman, G.P. Anderson, V.C. Sundar, F.V. Mikulec, M.G. Bawendi, Self-assembly of CdSe-ZnS quantum dot bioconjugates using an engineered recombinant protein, J. Am. Chem. Soc. 122 (2000) 12142–12150.

[8] S.A. Weston, C.R. Parish, New fluorescent dyes for lymphocyte migration studies. Analysis by flow cytometry and fluorescence microscopy, J. Immunol. Methods 133 (1990) 87–97.

[9] A.B. Lyons, C.R. Parish, Determination of lymphocyte division by flow cytometry, J. Immunol. Methods 171 (1994) 131–137.

[10] M. Bruchez Jr., M. Moronne, P. Gin, S. Weiss, A.P. Alivisatos, Semiconductor nanocrystals as fluorescent biological labels, Science 281 (1998) 2013–2016.

[11] W.C. Chan, S. Nie, Quantum dot bioconjugates for ultrasensitive nonisotopic detection, Science 281 (1998) 2016–2018.

[12] X. Gao, W.C. Chan, S. Nie, Quantum-dot nanocrystals for ultrasensitive biological labeling and multicolor optical encoding, J. Biomed. Opt. 7 (2002) 532–537.

[13] E.R. Goldman, E.D. Balighian, H. Mattoussi, M.K. Kuno, J.M. Mauro, P.T. Tran, G.P. Anderson, Avidin: a natural bridge for quantum dot–antibody conjugates, J. Am. Chem. Soc. 124 (2002) 6378–6382.

[14] D. Gerison, F. Pinaud, S.C. Williams, W.J. Parak, D. Zanchet, S. Weiss, A.P. Alivisatos, Synthesis and properties of biocompatible water-soluble silica-coated CdSe/ZnS semiconductor quantum dots, J. Phys. Chem. 105 (2001) 8861–8871.

[15] I.L. Medintz, A.R. Clapp, H. Mattoussi, E.R. Goldman, B. Fisher, J.M. Mauro, Self-assembled nanoscale biosensors based on quantum dot FRET donors, Nat. Mater. 9 (2003) 630–638.

[16] E.R. Goldman, G.P. Anderson, P.T. Tran, H. Mattoussi, P.T. Charles, J.M. Mauro, Conjugation of luminescent quantum dots with antibodies using an engineered adaptor protein to provide new reagents for fluoroimmunoassays, Anal. Chem. 74 (2002) 841–847.

[17] K. Hanaki, A. Momo, T. Oku, A. Komoto, S. Maenosono, Y. Yamaguchi, K. Yamamoto, Semiconductor quantum dot/albumin complex is a long-life and highly photostable endosome marker, Biochem. Biophys. Res. Commun. 302 (2003) 496–501.

[18] J.K. Jaiswal, H. Mattoussi, J.M. Mauro, S.M. Simon, Long-term multiple color imaging of live cells using quantum dot bioconjugates, Nat. Biotech. 21 (2003) 47–51.

[19] H. van Dekken, A. Hagenbeek, J.G. Bauman, Detection of host cells following sex-mismatched bone marrow transplantation by fluorescent in situ hybridization with a Y-chromosome specific probe, Leukemia 10 (1989) 724–728.

[20] R. Rizzuto, M. Brini, P. Pizzo, M. Murgia, T. Pozzan, Chimeric green fluorescent protein as a tool for visualizing subcellular organelles in living cells, Curr. Biol. 5 (1995) 635–642.

[21] C. Kaether, H.H. Gerdes, Visualization of protein transport along the secretory pathway using green fluorescent protein, FEBS Lett. 369 (1995) 267–271.

[22] Y.T. Lim, S. Kim, A. Nakayama, N.E. Stott, M.G. Bawendi, J.V. Frangioni, Selection of quantum dot wavelengths for biomedical assays and imaging, Mol. Imaging 2 (2003) 50–64.

[23] A. Hayashi, T. Nakanishi, J. Kunisawa, M. Kondoh, S. Imazu, Y. Tsutsumi, K. Tanaka, H. Fujiwara, T. Hamaoka, T. Mayumi, A novel vaccine delivery system using immunopotentiating fusogenic liposomes, Biochem. Biophys. Res. Commun. 261 (1999) 824–828.

[24] T. Nakanishi, A. Hayashi, J. Kunisawa, Y. Tsutsumi, K. Tanaka, Y. Yashiro-Ohtani, M. Nakanishi, H. Fujiwara, T. Hamaoka, T. Mayumi, Fusogenic liposomes efficiently deliver exogenous antigen through the cytoplasm into the MHC class I processing pathway, Eur. J. Immunol. 30 (2000) 1740–1747.

[25] J. Kunisawa, T. Nakanishi, I. Takahashi, A. Okudaira, Y. Tsutsumi, K. Katayama, S. Nakagawa, H. Kiyono, T. Mayumi, Sendai virus fusion protein mediates simultaneous induction of MHC class I/II-dependent mucosal and systemic immune responses via the nasopharyngeal-associated lymphoreticular tissue immune system, J. Immunol. 167 (2001) 1406–1412.

[26] M. Harada-Shiba, K. Yamauchi, A. Harada, I. Takamisawa, K. Shimokado, K. Kataoka, Polyion complex micelles as vectors in gene therapy–pharmacokinetics and in vivo gene transfer, Gene Ther. 9 (2002) 407–414.

[27] M.E. Akerman, W.C. Chan, P. Laakkonen, S.N. Bhatia, E. Ruoslahti, Nanocrystal targeting in vivo, Proc. Natl. Acad. Sci. USA 99 (2002) 12617–12621.

[28] D.R. Larson, W.R. Zipfel, R.M. Williams, S.W. Clark, M.P. Bruchez, F.W. Wise, W.W. Webb, Water-soluble quantum dots for multiphoton fluorescence imaging in vivo, Science 300 (2003) 1434–1436.

特集にあたって

A new technology developing diagnoses and evaluation of therapy by bioimaging——Introduction

鈴木和男
Kazuo Suzuki
国立感染症研究所生物活性物質部，日本バイオイメージング学会会長

治療や医薬の安全性が重視されている今日，安全で経済性の高い医薬の提供，非侵襲性の診断法や治療判定，医薬・診断の安全性の評価など，これまでにない医療分野での新しい技術の開発が要望されている．一方，治療薬の開発には莫大な費用がかかり，ひいては薬価へそれがはねかえってくる．また，臨床試験にも莫大な費用と時間がかかり，審査基準も厳しい状況から，多くの日本の製薬企業は海外で臨床試験，審査をしているともいわれている．このような現状のなかにあって，あらたな診断法，治療評価法を開発し，的確で簡便な方法を利用した日本発信のテクノロジーを使った医療分野の発展を考えなくてはならない時代にさしかかっている．

このような状況のなか，昨年(2003)から今年(2004)はじめにかけて“バイオイメージングによる医療応用をめざした”シンポジウムを3回企画した[1-3]．このときのテーマをもとに，医療応用に関連するバイオイメージングの研究者に，今回の特集のメインテーマ“バイオイメージングが切り開くあらたな診断・治療評価技術”に沿って執筆してもらうことにした．

これからの新しい“診断法”や“治療評価”に，“ナノテクノロジー”で開発された微小な分子や，微細な構造解析法も使ってバイオイメージングのテクノロジーを利用することが日常的になってきている．つまりイメージング技術とナノテクノロジーとの融合による医学・生物の現象解析が不可欠になりつつあることを物語っている．その意味で，バイオイメージング技術は医療の先端技術であり，その医用応用への研究が急速に進展しつつある．このように，バイオイメージングの技術は医療分野での応用に取り入れられる状況になっている．その背景には医学・生物学において“みる技術”を活用した“バイオイメージング”が定着していることがあげられる．

そこで今回は，新しいテクノロジーの創出による治療法・診断の方法の基礎や新しい治療法の開発などに主眼をおいた特集を企画した．

文献

1) 日本バイオイメージング学会・他：シンポジウム，バイオイメージングとナノテクノロジー．東京，2003年2月20～21日．
2) 日本バイオイメージング学会・他：シンポジウム，ナノとバイオの融合学理構築，産業基盤形成．松島，2003年9月10～11日．
3) 日本バイオイメージング学会・他：シンポジウム，バイオイメージング—最近の進歩と医療への応用．東京，2004年1月9日．

血管炎初期反応のイメージング

In vivo imaging of MPO-ANCA related glomerulonephritis in mouse

長尾朋和(写真)　鈴木和男
Tomokazu Nagao and Kazuo Suzuki
国立感染症研究所生物活性物質部

◎腎炎，SLE，リウマチをはじめとする難治性血管炎は，自己免疫疾患などの免疫異常による好中球の活性化や好中球自己抗体と連動して進行するものと予想されている．著者らはそのなかでもANCA陽性の急速進行性糸球体腎炎に注目し，その炎症初期に起こるであろうと考えられる血管傷害について，腎血流の *in vivo* イメージング手法を用いて検討した．本稿ではその手法と結果について，概略を解説したい．

Key word：好中球自己抗体，糸球体腎炎，*in vivo* イメージング

MPO-ANCA陽性糸球体腎炎

Anti-neutrophil cytoplasmic antibody(ANCA)陽性の急速進行性糸球体腎炎は，わが国においてはmyeloperoxidase(MPO)を抗原とするMPO-ANCAの抗体価が上昇するタイプが多くみられる[1]．MPO-ANCA陽性の半月体形成性腎炎は糸球体基底膜に補体や免疫グロブリンの沈着を認めないpauci-immune型であることが特徴であるが，現在のところ，このような特徴を示し，かつMPO-ANCA単独で半月体形成性腎炎を誘導できる動物モデルはXiaoらの報告[2]を除いて存在しない．MPOがMPO-ANCAの抗原になっていることはMPO欠損マウスで明らかにされており[3]，ほかにもリスクファクターとなるようなサイトカインやケモカインが報告されている[4,5]が，これらとMPO-ANCAがどのように血管炎の発症・進展にかかわっているのか，いまだ明らかになっていないのが現状である．また，上記のように最適な動物モデルが存在しないため，これまでMPO-ANCAに関して得られた知見の多くは *in vitro* における実験によるものであった．しかし，今後のより詳細な発症メカニズムの検討や，グロブリン治療[6]などの治療効果を含めた解析を行ううえでは，*in vivo* における解析手法の確立が重要視されてきている．

腎微小血管傷害を起こす誘導型モデルマウス

著者らも，MPO-ANCAとしてpolyclonal rabbit anti-mouse MPO antibody(anti-mMPO)のみをC57BL/6マウスに静脈内投与した場合，anti-mMPOのみではマウスに腎炎を発症させることが不可能であった．そこで，モデルには *Candida albicans* 由来糖ペプチドCAWS，polyclonal rabbit anti-mouse MPO antibody(anti-mMPO)およびfMet-Leu-Phe(FMLP)の3種類の物質を組み合わせて用いた．CAWSは大野らによって作製されたもので，比較的大きいサイズの動脈に血管炎を誘導することが知られている[7,8]．また，FMLPは好中球走化性因子であり，これを用いて好中球を活性化することができる．そこで，これらを静脈内投与することで，急性的に腎微小血管傷害を起こす誘導型モデルマウスの確立をめざした．最終的なプロトコールはC57BL/6マウス(雄，9週齢)にCAWS(150 μg/mouse)を静脈内投与し，その3

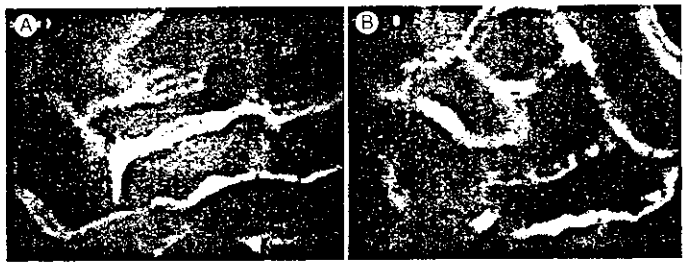

図1　コントロールマウス(A)およびCAWS+anti-mMPO+FMLPを投与したマウス(B)の腎表面血流

FITC-dextranによって蛍光を発し，白くみえる網目状の部分が毛細血管で，血管以外の暗い部分は尿細管である．コントロールマウスでは血流速度が速いため，個々の血球細胞を確認することができないが，腎炎を誘導したマウスでは血流が停止しつつあるため，赤血球などが黒いスポットとして確認できる．

時間後にanti-mMPO(1 mg/mouse)を，加えて5日後にfMet-Leu-Phe(FMLP，10^{-8}mol/mouse)を静脈内投与するものである．このモデルマウスは慢性的な腎炎を引き起こすものではないが，FMLPの投与から一過性の蛋白尿などの特徴を示し，さらに糸球体には微小血栓もみられるなど，糸球体毛細血管に何らかの傷害を与えるものであった．

In vivo イメージング

著者らはこのモデルマウスの評価手段として，*in vivo* イメージングを利用した．とくに血管炎のように血管がおもな傷害の場となる場合，血流のような生体内のダイナミックな変化をとらえることが可能な*in vivo* イメージング技術は非常に有用である．また，組織学的には変化が確認できないような，炎症における比較的初期段階を評価するためにも最適な手法といえる．これまでにも透過光による観察が容易な腸間膜微小循環系を対象とした研究が行われてきたが，実質臓器レベルにおいても臓器自体の厚みのために光透過が非常に悪いものの，蛍光物質をトレーサーとした臓器表層の血流観察が可能であり，これによって多くのあらたな知見が報告されてきている．著者らが観察対象とした腎は臓器全体に毛細血管がはりめぐらされており，血液による光吸収の影響が大きいため，糸球体毛細血管の血流状態を観察することは非常に困難であった．しかし，リアルタイム共焦点顕微鏡[9]や2光子励起顕微鏡[10]などを用いて糸球体血流を可視化することが可能になってきている．

著者らの用いた実験系は通常の蛍光顕微鏡観察と同様で非常にシンプルであり，モデルマウスの血流は蛍光物質FITC-dextranを用いて可視化することとした．FITC-dextranの分子量は約280,000であり，通常の機能を有した血管であれば，血管外に漏れ出すことはない．すなわち，蛍光顕微鏡観察を行ったときに血漿のみが蛍光を発することとなる．また，特殊な細胞以外にはほとんど取り込まれないため，赤血球などは蛍光を発しない．実際の手順としては，麻酔下のマウスにFITC-dextranを尾静脈投与した後，背部を切開し腎のみを露出させた後，これを生存状態のまま倒立顕微鏡下において蛍光観察した．また，観察中はヒーティングプレートを用いて37℃に保ち，さらに生理食塩水を用いて臓器の乾燥を防いだ．この方法によって腎表面を流れる尿細管周囲毛細血管の可視化が可能となり，また腎表面より50 μm以内に存在する糸球体であれば，その毛細血管を可視化することも可能となった．しかし，残念ながら腎表面より50 μm以内に存在する糸球体は非常に少なく，その後の解析に供する量の映像は得られなかった．そこで，観察対象となる血管は尿細管周囲毛細血管とし，その血流動態をDVDレコーダーで録画した後，画像解析を行った．

モデルマウスにおける血流の悪化

この観察手法を用いて確立した誘導型モデルマ

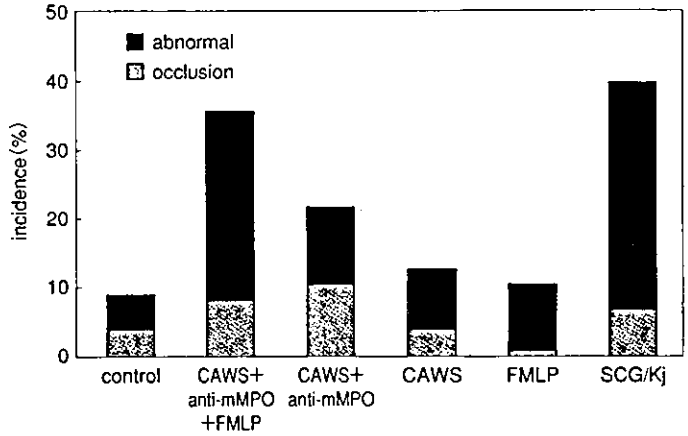

図 2　各投与条件における血流が停止した血管(occulusion)と異常な血流がみられる血管(abnormal)の割合

CAWS, FMLP, anti-mMPO の 3 種類すべてを投与した場合において顕著な血流停止，異常血流が観察され，糸球体腎炎の自然発症マウスである SCG/Kj マウスにおいても同程度の血流停止や異常血流がみられた．

ウスおよび無処理のコントロールマウスにおける腎血流動態を比較したところ，モデルマウスにおいて顕著な腎微小循環の悪化が観察された(図 1)．具体的には血流速度の低下・血流停止・血液の逆流などの現象が観察され，CAWS または FMLP 単独投与の場合と比較し，anti-mMPO を投与した場合に血流停止(occlusion)が誘発され(観察した血管の約 10%)，さらに 3 種類すべてを投与した場合には広範囲にわたる腎表面血流の悪化(abnormal)が観察された(観察した血管の約 30%)(図 2)．このような腎表面血流の悪化は，糸球体腎炎の自然発症マウスである SCG/Kj マウスにおいても同様にみられた．さらに，この腎微小循環の悪化には血管内皮への白血球の接着を伴ったものもみられ，anti-mMPO を用いたこの腎炎誘導モデルにおいては MPO の関与が予想されることから，観察された白血球のなかでもとくに MPO を発現している好中球が炎症における重要な役割を担っているものと考えられる．

おわりに

血管炎初期反応のイメージングとして，とくに糸球体腎炎を対象とした *in vivo* イメージングを紹介した．本手法により血管内で起こっている現象をリアルタイムにとらえることが可能となり，その結果，MPO-ANCA が関連する血管炎の初期において，内皮細胞への白血球の接着とそれによる血流の悪化がみられることが明らかとなった．近年のコンピュータ画像処理技術の進歩によって顕微鏡の性能も向上してきており，上記の高速共焦点顕微鏡や 2 光子励起顕微鏡など，*in vivo* イメージングにより適した顕微鏡も開発されてきている．今後，これらの顕微鏡技術を用いた新しい知見が期待される．

なお，本研究は厚生労働科研費により行われた．

文献

1) 中林公正，土岐岳士：ANCA 関連血管炎の臨床像．医学のあゆみ，**206**：130-132，2003．
2) Xiao, H. et al.：Antineutrophil cytoplasmic autoantibodies specific for myeloperoxidase cause glomerulonephritis and vasculitis in mice. *J. Clin. Invest.*, **110**：955-963, 2002.
3) Ishida-Okawara, A. et al.：Contribution of myeloperoxidase to coronary artery vasculitis associated with MPO-ANCA production. *Inflammation*, **25**：381-387, 2001.
4) Cockwell, P. et al.：Interleukin-8：A pathogenic role in antineutrophil cytoplasmic autoantibody-associated glomerulonephritis. *Kidney Int.*, **55**：852-863, 1999.
5) Arimura, Y. et al.：Serum myeloperoxidase and serum cytokines in anti-myeloperoxidase antibody-associated glomerulonephritis. *Clin. Nephrol.*, **40**：

256-264, 1993.
6) Jayne, D. R. W. et al. : Intravenous immunoglobulin for ANCA-associated systemic vasculitis with persistent disease activity. *Q. J. Med.*, **93** : 433-439, 2000.
7) 大野尚仁：血管炎を誘導する真菌糖蛋白質の免疫活性化. 医学のあゆみ, **206** : 150-152, 2003.
8) Ohno, N. : Chemistry and biology of angiitis inducer, *Candida albicans* water-soluble mannoprotein-β-glucan complex(CAWS). *Microbiol. Immunol.*, **47** : 479-490, 2003.
9) Oyanagi-Tanaka, Y. et al. : Real-time observation of hemodynamic changes in glomerular aneurysms induced by anti-Thy-1 antibody. *Kidney Int.*, **59** : 252-259, 2001.
10) Dunn, K. W. et al. : Functional studies of the kidney of living animals using multicolor two-photon microscopy. *Am. J. Physiol. Cell Physiol.*, **283** : C905-C916, 2002.

腎臓血管傷害のイメージング

国立感染症研究所生物活性物質部*，東京理科大学理工学部** 長尾 朋和*，村山 研*,**，越尾 修*
東京薬科大学薬学部#，東邦大学医学部大橋病院** 大野 尚仁#，三浦 典子#，高橋 啓**
オタゴ大学(ニュージーランド)† 馬渕 綾子†，南谷 晴之††
慶應義塾大学大学院基礎理工学部†† 鈴木 和男*,**

要 旨

腎炎，動脈炎，SLEなどの難治性血管炎は，好中球自己抗体(anti-neutrophil cytoplasmic antibodies；ANCA)が血清中に検出される自己免疫疾患で，免疫異常や好中球活性化と連動して進行するものと予想されている。好中球活性化の関与については，病理組織切片の観察の知見によっているが，生体ではどのような状況で活性化されているかは明らかではない。おそらく，*in vivo*での血管内部は，血管炎に伴って，血圧・血流速度などの血行力学的因子が変化していると想像される。これらの血流因子の変化を*in vivo*で解析し，血管傷害の要因を検証することが必要である。この方法には，顕微鏡を用いた*in vivo*の生存状態で，臓器微小循環血流を観察して，血流のパラメーターを定量的に評価することが必要である。この方法により，腎炎において重要な働きを担っているものと思われる好中球の動態も*in vivo*での観察・解析が可能である。そこでわれわれは，腎炎の発症・進展におけるANCAおよび好中球の役割を明らかにするために，腎炎モデルマウスの構築およびin vivoイメージング観察を行った。その結果，*Candida albicans*由来糖ペプチド(CAWS)，rabbit anti-mouse myeloperoxidase(anti-mMPO)およびfMet-Leu-Pheによって腎血管傷害を誘導したC57BL/6マウスでは，血流速度の低下，血流停止，血液の逆流などが観察され，最も顕著な場合，広範囲にわたる腎表面血流の停止も観察された。さらに，これらの現象には血管内皮への白血球の接着も観察された。本腎炎誘導モデルにおいては，myeloperoxidase(MPO)が関連していることから，観察された白血球のなかでも特に好中球が炎症における重要な役割を担っているものと考えられる。本血管炎誘導モデルにおいて開発したin vivoイメージングの評価法は，血管炎の進行によって誘発される多臓器不全の治療法の開発や，治癒機転および発症機構を解析するうえで有用であることを示した。

I. 緒 言

難治性血管炎は，腎炎，動脈炎やSLEなどとして顕れ，その要因の1つにANCAが，血清中に増加することが明らかにされてきている[1)-4)]。このように，難治性血管炎には，自己免疫疾患などの免疫異常が関与している[5)]。また，ANCAの対応分子の主なものが，好中球顆粒酵素のprotease-3(PR-3)やMPOであることから，好中球の活性化が発症や病態に関与していることが予想される[6)7)]。

また，生体防御機能の不全は，好中球や免疫細胞の機能破綻やそれによるサイトカインの異常なネットワークのかく乱を誘導し，種々の臓器障害をもたらす。血管内皮細胞は，サイトカインと活性化白血球の攻撃にさらされ，また，臓器内での異常反応の前線となる。特に，好中球活性化は，難治性血管炎の発症およびその要因になっていることが強く示唆されており，好中球の殺菌酵素であるMPOがMPO-ANCAの抗原になっていることをわれわれは明らかにした[8)]。すなわち，ANCAが好中球を活性化し，血管炎の発症に関わっている可能性を示唆した[9)10)]。

一方，血管炎の病初期には，病理組織切片の観察から好中球が浸潤していることから裏付けられている。しかし，病理所見による*in vitro*の観察は，生体の生きたままでの観察ではないことから，生体での状況をそのまま解析することはできない。血管炎に伴って，生体の血管内部では，血圧・血

流速度などの血行力学的因子が変化していると推定されるが，*in vitro*では，これらの因子の変化をとらえることはかなり困難である。しかしながら，これらの因子が血管傷害に影響を及ぼすかを検証することが必要である。そこで，顕微鏡を用いた*in vivo*の観察システムより，生存状態で臓器微小循環血流を観察して，これらのパラメーターを定量的に評価することが必要である。さらに，重要な働きを担っているものと推定されている好中球の血管内部での動態も，本システムを使って*in vivo*での観察・解析をすることも重要である。一方，本システムの開発には，動物モデルが必要である。そこで，カンジダ菌成分Candida albicans derived substances (CADS)の接種による好中球抗体MPO-ANCAが血中に増加する冠状動脈炎モデルを用いた[11]。また，カンジダ菌外成分CAWSも血管炎を強く誘導することが可能である。

そこで，本研究では，CAWSによる腎傷害モデルマウスを作製し，本モデルマウスにより，in vivoイメージング法を開発した。それにより，腎炎の発症・進展におけるANCAおよび好中球の役割を検討した。

Ⅱ．研究方法

①多臓器不全関連血管炎モデルマウスの調整：*C. albicans*由来物質CAWSを投与して誘導した。

②in vivo イメージング：C57BL/6マウス(オス，9週齢)にCAWS(150 mg/mouse)をiv投与し，3時間後にanti-mMPO(rabbit anti-mouse myeloperoxidase，1 mg/mouse)をiv投与した。5日後，同様にCAWSとanti-mMPOを投与した後，fMet-Leu-Phe(FMLP，10^{-8} mol/mouse，細菌由来トリペプチド)をiv投与し，その3日後に腎表面における血流状態を観察した。血流の可視化にはFITC-dextranを用い，各マウスの腎表面における尿細管周囲毛細血管の血流を観察した。観察される血流動態は顕微鏡に接続したビデオカメラで撮影し，DVDに録画した。

Ⅲ．結　果

腎血管傷害を誘導するためにCAWS，anti-mMPOおよびfMet-Leu-Pheを投与し，腎臓表面血管のin vivoイメージングにより，血流速度の低下，血流停止，血液の逆流を観察・解析した。

①PBS投与のコントロールマウスでの腎臓血管の血流を観察した(図1)。

図1．コントロールマウスの腎血管のin vivoイメージング

②CAWS，anti-mouseMPOおよびfMet-Leu-Pheの投与による腎微小循環傷害のin vivoイメージング。

CAWS，anti-mouseMPOおよびfMet-Leu-Pheの投与によって，腎微小循環が悪化する様子がin vivoイメージングにより観察された(図2)。CAWSの投与によって，冠状動脈炎が誘導された。その頻度は，100%近い値を示した。この濃度以上の投与は，全身性の多臓器不全様ショックにて死亡した。また，in vivoイメージングの解析では，血流速度の低下，血流停止，血液の逆流が観察され，腎表面血流の停止がみられた(図2)。

③血流遮断と血管内皮細胞への白血球接着。

腎臓表面血管の流速の変化も，CAWS＋anti-mouseMPO＋fMet-Leu-Pheのときに悪化した。血流速度の低下・血流停止・血液の逆流などの現象が観察され，CAWSまたはFMLP単独投与の場合と比較し，両者に加えてanti-mMPOを投与した場合に血流停止が誘発され(観察した血管の約10%)，広範囲にわたる腎表面血流の悪化が観察された(約30%)。さらに，この腎微小循環の悪化には血管内皮細胞への白血球の接着を伴ったものもみられた(図3)。

C57BL/6マウスにCAWS，anti-mMPOおよびfMet-Leu-Pheを投与して誘導される腎血管傷害をin vivoイメージングにより，血流速度の低下，血流停止，血液の逆流を観察した。また，広範囲にわたる腎表面血流の停止も観察した。さらに，これらの現象には血管内皮への白血球の接着を伴ったものも観察された。

Ⅳ．考　察

CAWSによって，冠状動脈炎が100%近く発症し，投与量の増加により，多臓器不全様ショックで死亡した。この血管炎誘導モデルにおいては，*C. albicans*由来糖ペプチドCAWSが，MPOおよびMPO-ANCA産生と発症誘導に不可欠であることから，CAWSなどの真菌由来分子がサイトカインと連動して好中球を活性化して，多臓器不全様の症状を誘発する役割を担っているものと考えられる。その結果，急速な血管炎を誘発し，ひいては，多臓器不全をきたしたと考えられる。そのCAWSに加え，anti-mouseMPOおよびfMet-Leu-Pheを投与し，in vivoイメージングすることにより，血流速度の低下，血流停止，血液の逆流が観察され，腎表面血流の停止や血管内皮への白血球の接着も

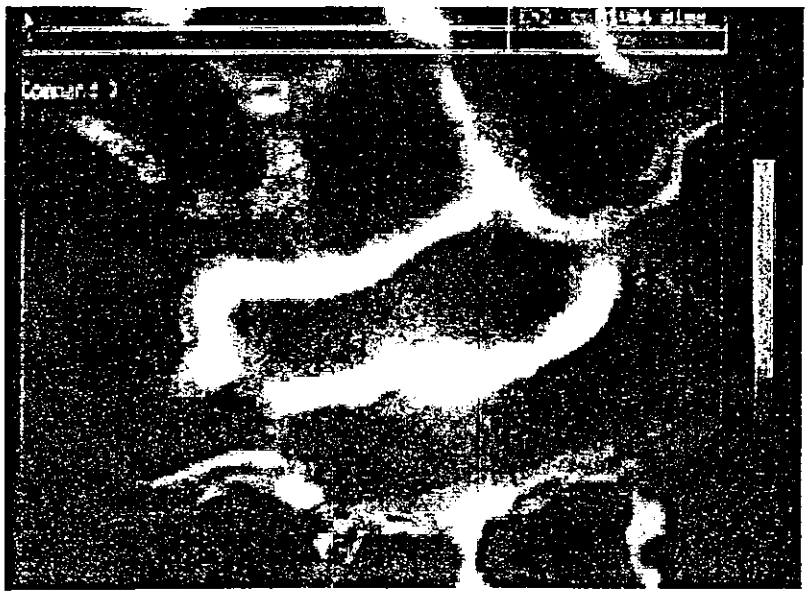

図2．CAWS誘導の腎血管傷害in vivoイメージング
CAWS＋anti-mMPO＋FMLP

図3．CAWS誘導の腎血管傷害in vivoイメージングにおける血管内皮への白血球の接着

みられた。この*in vivo*での現象が，腎血管傷害の誘導を説明できると思われるが，分子機構との関係を明らかにする必要があり，さらに検討する必要がある。CAWSおよびanti-mMPOによって誘導される腎微小血管傷害誘導モデルを用いたin vivoイメージングの解析から以下のような推論が得られた。まずCAWSによって好中球数の増加・好中球活性化が誘発される。この状態において投与された好中球自己抗体(anti-mMPO)は，活性化によって細胞膜表面へ移行したMPOと複合体を形成し，さらなる好中球の活性化・血管内皮細胞への接着・活性酸素種の産生を引き起こすと考えられる。このことから，白血球のなかでも特に好中球が炎症における重要な役割を担っているものと推察される。また，このin vivoイメージング解析による評価法は，CAWS誘導血管炎やSCG/Kjマウスなどの腎炎モデル[12)-14)]での発症機構の解析に有用であり，本システムの利用が期待される。また，血管炎の治療法[15)-17)]の新しい評価系として有用であると思われる。このように，微小血管傷害を生体内で観察するシステムは，血管炎や多臓器不全の治療法の評価や治癒機構の解析として，今後の利用が期待される。

文　献

1) Jennette JC, Falk RJ：Antineutrophil cytoplasmic autoantibodies and associated diseases：a review. Am J Kidney Dis 15：517－529, 1990
2) Suzuki K：Neutrophil functions of patients with vasculitis related to MPO-ANCA. Int J Hematol 74：134－143, 2001
3) Savage COS, Winearls CG, Jones SJ, et al：Prospective study of radioimmunoassay for antibodies against neutrophil cytoplasm in diagnosis of systemic vasculitis. Lancet 1：1389－1393, 1987
4) Cohen Tervaert JW, Goldschmeding R, Elema JD, et al：Autoantibodies against myeloid lysosomal enzymes in crescentic glomerulonephritis. Kidney Int 37：799－806, 1990
5) Harper JM, Thiru S, Lockwood CM, et al：Myeloperoxidase autoantibodies distinguish vasculitis mediated by anti-neutrophil cytoplasm antibodies from immune complex disease in MRL/Mp-lpr/lpr mice：a spontaneous model for human microscopic angitis. Eur J Immunol 28：2217－2226, 1998
6) Tomizawa K, Mine E, Fujii A, et al：A panel set for epitope analysis of myeloperoxidase (MPO)-specific antineutrophil cytoplasmic antibody MPO-ANCA using recombinant hexamer histidine-tagged MPO deletion mutants. J Clin Immunol 18：142－152, 1998
7) Fujii A, Tomizawa K, Arimura Y, et al：Epitope analysis of myeloperoxidase (MPO) specific anti-